Its Detection, edited by Y.-H. Pao and A. Goldburg, Plenum Press, New York, 1969, p. 371.

[14] Fichtl, G. H., Camp, W., and Vaughan, W. W., "Detailed Wind and Temperature Profiles," *Clear Air Turbulence and Its Detection*, edited by Y.-H. Pao, and A. Goldburg, Plenum Press, New York, 1969, pp. 308–333.

[15] Mather, G. K., "Clear Air Turbulence Research Activities at the National Aeronautical Establishment," *Clear Air Turbulence and Its Detection*, edited by Y.-H. Pao, and A. Goldburg, Plenum Press, New York, 1969, p. 271.

[16] Blackman, R. B. and Tukey, J. W., *The Measurement of Power Spectra*, Dover, New York, 1958.

[17] Zimmerman, S. P. and Loving, N. V., "Turbulent Dissipation and Diffusivities in the Stratosphere," *CIAP Monograph*, Vol. 1: The Natural Stratosphere, Appendix D-2, 1973.

[18] Hinze, J. O., *Turbulence*, McGraw-Hill, New York, 1959, p. 192.

[19] Phillips, O. M., "On the Bolgiano and Lumley-Shur Theories of the Buoyancy Subrange," *Atmospheric Turbulence and Radio Wave Propagation*, Publishing House "Nauka," Moscow, USSR, 1967, p. 121.

AUGUST 1974 AIAA JOURNAL VOL. 12, NO. 8

Coupled Nongray Radiating Flow about Ablating Planetary Entry Bodies

KENNETH SUTTON*
NASA Langley Research Center, Hampton, Va.

A method of solution for the fully coupled radiating gas flow about an ablating, planetary entry body is developed and applied to Venusian entries. The method couples an inviscid flow solution and a boundary-layer solution (laminar or turbulent) in which the divergence of the radiative flux is included in the energy equation for the solution of each gas layer. The treatment of radiation includes molecular band, continuum, and line transitions with a detailed frequency dependence of the absorption coefficient. Results are presented at typical conditions for unmanned, scientific probes during Venusian entries. These results show that the radiative flux toward the body is attenuated in the boundary layer at downstream regions of the body as well as at the stagnation point and that, even when radiation absorption by ablation products is accounted for, the radiative heating rates along the downstream regions of the body can, under certain conditions, exceed the stagnation-point values. It is also shown that, for Venusian entry, the spectral distribution of radiative flux and the magnitude of radiation absorption by ablation products depend strongly on entry velocity, and that the state of the boundary layer (i.e., laminar or turbulent) can significantly influence the amount of ablation product absorption or emission that occurs in various spectral regions.

Nomenclature

A, B, C, D, E = parameters defined by Eqs. (11–15)
C_2, C_3 = parameters defined by Eqs. (25) and (26)
c_p = specific heat
$\bar{c}_p$ = specific heat parameter defined by Eq. (34)
$\bar{D}$ = self-diffusion coefficient of a reference species
F^R = divergence of radiative flux defined by Eq. (16)
F_j = diffusion factor of jth chemical species
H = total enthalpy, $h+u^2/2$, in Eq. (30)
h = enthalpy
$\bar{h}$ = enthalpy parameter defined by Eq. (34)
j_i = diffusional mass flux of chemical element i
K = body curvature parameter defined by Eq. (19)
$\bar{K}_i$ = mass fraction of chemical element i
k = thermal conductivity
M = molecular weight
m_a = ablation rate of the heat shield
P_1, P_3 = thermodynamic variables defined by Eqs. (20) and (21)
P = pressure
q^C = convective heat flux, see Eq. (33)
q^R = radiative heat flux
Re_θ = momentum thickness Reynolds number for boundary layer
Rn = nose radius of body at $s = 0$, see Fig. 3
r = radial distance from axis of symmetry of body, see Fig. 3
r_b = body radius from axis of symmetry, see Fig. 3
S, Y, T = transformed s, y, t coordinates, defined by Eq. (6)
s, y = body-oriented coordinates, see Fig. 3
$\bar{T}$ = temperature
t = time
u, v = velocity components, see Fig. 3
V_∞ = freestream velocity
V_e = entry velocity
W = weight of entry probe
W/C_dA = ballistic coefficient
$\bar{x}_j$ = mole fraction of chemical species j
$\bar{Z}_j$ = quantity for jth chemical species defined by Eq. (34)
$\bar{Z}_i$ = quantity for ith chemical element defined by Eq. (34)
α_{ij} = mass fraction of chemical element i in chemical species j
β = angle between shock and body, see Fig. 3
γ_e = entry angle
δ = shock standoff distance of inviscid layer
δ^* = boundary-layer displacement thickness defined by Eq. (2)
δ^t = total thickness of shock layer defined by Eq. (1)
θ = body angle, see Fig. 3
θ_c = cone half angle for a spherically capped, conical body
λ = curvature parameter defined by Eq. (17)
λ_δ = value of λ at $y = \delta$, see Eq. (18)
μ = viscosity
μ_1, μ_2 = parameters defined by Eq. (34)
ρ = density
$\rho\varepsilon_d$ = turbulent eddy diffusivity
$\rho\varepsilon_h$ = turbulent eddy conductivity
$\rho\varepsilon_m$ = turbulent eddy viscosity
τ_w = aerodynamic shear at the wall
ϕ = azimuth angle, see Fig. 3

Presented as Paper 73-672 at the AIAA 6th Fluid and Plasma Dynamics Conference, Palm Springs, Calif., July 16–18, 1973; submitted July 31, 1973; revision received February 20, 1974.

Index category: Radiatively Coupled Flows and Heat Transfer.

* Aero-Space Technologist, Gas Radiation Section, Advanced Entry Analysis Branch, Space Systems Division. Member AIAA.

Subscripts

e = boundary-layer edge
w = body wall
∞ = freestream conditions
ν = radiation frequency

Introduction

FULLY coupled, radiating gas flow solutions with ablation product effects are available for the stagnation point of bodies for Earth re-entry.[1] The results show that the boundary layer with ablation products injection can absorb radiation emitted from the higher temperature regions of the flowfield thus reducing the radiative heating to the body. However, comparable solutions for the downstream region of entry bodies and for entries into other planets have not been available. Valid solutions for the downstream regions of ablating entry bodies are needed since most of the heat-shield surface and weight is downstream of the stagnation point.[2] These downstream solutions should include a turbulent boundary layer since most planetary bodies will experience turbulent flow during entry. The results for an inviscid, radiating flowfield solution about blunted, conical bodies for Earth re-entry have shown that the radiative heating to the cone's flanks can exceed the radiative heating to the stagnation region of the body.[3] There is a need for solutions of the radiating flowfield in gaseous atmospheres other than air because of the increased interest in exploration of the planets (Venus, Jupiter, etc.) by entry probes. A proposed mission to Venus (Pioneer Venus) is the first planetary entry mission in which radiative heating is a dominant feature of the aerothermodynamic environment and a detailed analysis is needed to evaluate the heat-shield requirements of the entry probes.

In the present study, a method is presented for the solution of a fully coupled, radiating gas flowfield about an ablating, planetary entry body and is applied to Venusian entry. The results presented are for the steady-state ablation of carbon-phenolic heat shields at typical conditions during entry for unmanned, scientific probes into the Venusian atmosphere.

Method of Analysis

The radiating flowfield about the entry body is separated into an outer layer where the inviscid flow equations are applicable and an inner viscous layer where the boundary-layer equations are applicable. The divergence of the radiative flux is included in the energy equation for the solution of each layer and the boundary layer is coupled to the inviscid shock layer by the radiative transport through both layers and by the boundary-layer displacement thickness. This coupling of the boundary-layer solution to the inviscid shock layer solution is illustrated by the temperature profile shown in Fig. 1. The inviscid flowfield

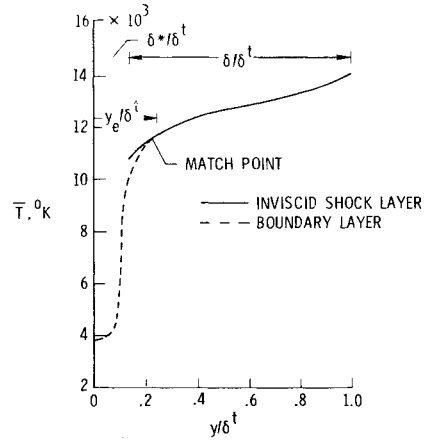

Fig. 1 Illustration of mating of boundary layer to inviscid layer.

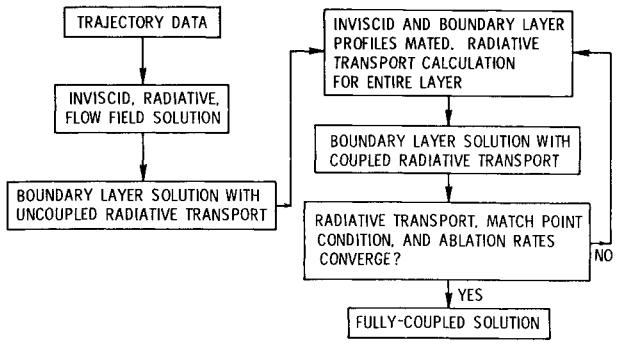

Fig. 2 Calculation procedure for the fully coupled, radiating, flowfield solution.

is displaced from the wall by the boundary-layer displacement thickness and the boundary-layer profiles are used out to the point where the boundary-layer edge values and their derivatives equal the inviscid layer values. For the boundary-layer solution, the radiative transport is calculated from the mated profiles for the entire layer. The total thickness of the flowfield now becomes

$$\delta^t = \delta + \delta^* \tag{1}$$

where δ is the thickness of the inviscid shock layer (shock standoff distance) and δ^* is the boundary-layer displacement thickness calculated from

$$\delta^* = \int_0^{y_e} \left(1 - \frac{\rho u}{\rho_e u_e}\right) dy + \frac{1}{\rho_e u_e r_b} \int_0^s (\rho v)_w r_b \, ds \tag{2}$$

The radiating, inviscid flowfield solution is calculated only once for the fully coupled solution; but an iteration is required to couple the boundary-layer solution to the inviscid flow solution because of inclusion of the radiative heat flux in the boundary layer and locating the boundary-layer edge in the inviscid flowfield. The boundary-layer solution is assumed not to affect the inviscid layer solution. The boundary conditions for the boundary-layer edge are the appropriate values and their derivatives at the match point in the inviscid flow solution and are not the values at the wall condition of the inviscid flow solution.

The calculation procedure for the fully coupled solution is shown in Fig. 2. The steps in the procedure are: 1) An inviscid, radiating solution is calculated from trajectory data. 2) A boundary-layer solution with uncoupled radiative transport is calculated using the inviscid wall values for the boundary-layer edge conditions. For steady-state ablation, the radiative heating to the wall is taken as the inviscid wall value. 3) The profiles from the inviscid solution and the boundary-layer solution are mated and the radiative transport is calculated for the entire layer. 4) A boundary-layer solution with coupled radiative transport is calculated using the values at the match point of the two layers for the boundary-layer edge values. 5) Steps 3 and 4 are repeated until the radiative transport through the layer, the match point condition, and the ablation rates (for steady-state ablation) converge. The inviscid flowfield and the boundary-layer solutions are for the flow around a body and the coupling of the two layers and the convergence of the final solution is applied at each location around the body.

A more detailed description of the components of the fully coupled solution is presented in Ref. 4. The solution is by numerical methods on a high-speed digital computer. The components, which are separate computer programs, are described briefly as follows.

Radiating, Inviscid Flowfield Solution

The computer program for the radiating, inviscid flowfield was developed in the present study. A second-order, time-asymptotic technique is used for the solution; therefore, the analysis is based on the equations of conservation of mass, momentum, and energy for unsteady flow. The conditions for which the present analysis

is carried out are that the flow is axisymmetric, inviscid, and nonconducting; the gas is in local thermodynamic and chemical equilibrium; the tangent slab approximation is valid for the radiative transport; and the shock wave is a discrete surface.

The equations in this section of the paper are nondimensionalized as follows: distance by Rn, time by Rn/V_∞, density by ρ_∞, pressure by $\rho_\infty V_\infty{}^2$, velocity by V_∞, enthalpy by $V_\infty{}^2$, and radiative flux by $\rho_\infty V_\infty{}^3$. Special symbols are not used to denote the nondimensionalization.

The conservation equations expressed in vector notation are

Continuity:

$$\partial\rho/\partial t+\nabla\cdot(\rho\mathbf{V})=0 \tag{3}$$

Momentum:

$$\partial\mathbf{V}/\partial t+\mathbf{V}\cdot\nabla\mathbf{V}-(1/\rho)\nabla p=0 \tag{4}$$

Energy:

$$\rho\,\partial h/\partial t+\rho\mathbf{V}\cdot\nabla h+\nabla\cdot\mathbf{q}^R-\partial p/\partial t-\mathbf{V}\cdot\nabla p=0 \tag{5}$$

The body-orientated coordinate system shown in Fig. 3 and the transformation

$$\left.\begin{aligned}T&=t\\S&=s\\Y&=y/\delta\end{aligned}\right\} \tag{6}$$

where

$$\delta=f(S,T)$$

are used to obtain the conservation equation used in the present study.

Continuity:

$$p_T=-\left[Ap_Y+\frac{u}{\lambda}p_S+P_3\left(\frac{\rho}{\lambda}u_s-Bu_Y+\frac{\rho}{\delta}v_Y+C\right)-\frac{F^R}{P_1\rho}\right] \tag{7}$$

S-momentum:

$$u_T=-\left(Au_Y+\frac{u}{\lambda}u_S-\frac{B}{\rho^2}p_Y+\frac{1}{\rho\lambda}p_S+D\right) \tag{8}$$

Y-momentum:

$$v_T=-\left(Av_Y+\frac{u}{\lambda}v_S+\frac{1}{\delta\rho}p_Y-E\right) \tag{9}$$

Energy:

$$h_T=-\left(Ah_Y+\frac{u}{\lambda}h_S-\frac{1}{\rho}p_T-\frac{A}{\rho}p_Y-\frac{u}{\rho\lambda}p_S+\frac{F^R}{\rho}\right) \tag{10}$$

where $(\ )_Y$, $(\ )_S$ and $(\ )_T$ indicate partial derivatives with respect to Y, S, and T, and

$$A=v/\delta-(Y/\delta)\delta_T-(uY/\delta\lambda)\lambda_\delta\tan\beta \tag{11}$$

$$B=(\rho Y/\delta\lambda)\lambda_\delta\tan\beta \tag{12}$$

$$C=(\rho u/r)\sin\theta+\rho v(K/\lambda+\cos\theta/r) \tag{13}$$

$$D=Kuv/\lambda \tag{14}$$

$$E=Ku^2/\lambda \tag{15}$$

$$F^R=(1/\delta)q_Y{}^R+q^R(K/\lambda+\cos\theta/r) \tag{16}$$

$$\lambda=1+K\delta Y \tag{17}$$

$$\lambda_\delta=1+K\delta \tag{18}$$

$$K=-d\theta/ds \tag{19}$$

$$P_1=1/\rho-(\partial h/\partial p)_\rho \tag{20}$$

$$P_3=(1/P_1)(\partial h/\partial\rho)_p \tag{21}$$

The values for the thermodynamic variables of ρ, P_1, and P_3 are determined by the conditions of chemical equilibrium for the gas with the specification of the elemental mass fractions of the gas and the two thermodynamic state variables of pressure and enthalpy. The continuity equation [Eq. (7)] is expressed in terms of pressure rather than density because density cannot be used as one of the specified thermodynamic state variables in the chemical equilibrium program used in the present study. The expression is obtained by combining the continuity equation and the energy equation with the aid of differential relations of the state equation in the functional form $h=f(\rho,p)$.

The concept of the time-asymptotic technique is to assume initial values for the flowfield variables and to follow the evolution of the flow in time until the flow contains a steady-state condition. The numerical method used in the present study to obtain a solution is based on the two-step method of MacCormack.[5,6] At time T the value of a variable is known at all locations in the flowfield. The advancement of a variable from time T to $T+\Delta T$ (one iteration) is given by

$$f(S,Y,T+\Delta T)=f(S,Y,T)+f_T{}^{\text{ave}}\Delta T \tag{22}$$

The symbol f represents the variable p,u,v, or h and $f_T{}^{\text{ave}}$ is an average time derivative between T and $T+\Delta T$. The time derivatives are calculated from the unsteady equations with finite differences used for the spatial derivations.

The solution for the location of the shock wave and the flowfield variables along the shock wave ($Y=1$) is by a method using a quasi-, one-dimensional, unsteady characteristic solution and the Rankine-Hugoniot equations for a moving shock.[4,7] The equation for a right running characteristic is

$$dY/dT=A+(P_3)^{1/2}/\delta \tag{23}$$

and the compatibility equation is

$$\frac{dv}{dT}+\frac{1}{\rho(P_3)^{1/2}}\frac{dp}{dT}=C_2+\frac{C_3}{\rho(P_3)^{1/2}} \tag{24}$$

where

$$C_2=-\left[(u/\lambda)v_S-E\right)] \tag{25}$$

$$C_3=-\left[\frac{u}{\lambda}p_S+P_3\left(\frac{\rho}{\lambda}u_S+C\right)-\frac{F^R}{P_1\rho}-P_3Bu_Y\right] \tag{26}$$

The compatibility equation must be satisfied between the shock point at time $T+\Delta T$ and an interior point at time T. The interior point is located from the characteristic equation. An iteration procedure is required for this solution by assuming a shock velocity, δ_T, and determining the flow variables behind the shock wave by the Rankine-Hugoniot equations for a moving shock. This procedure is applied around the body at each time step.

The radiative heat flux, the thermodynamic properties, and the solution of the Rankine-Hugoniot equations are calculated by a modified version of the computer program of Refs. 8 and 9.

Boundary-Layer Solution

The boundary-layer equations are for a nonsimilar, multicomponent laminar or turbulent boundary layer with mass injection, unequal diffusion coefficients, and arbitrary chemical species. The solution of the equations is by a numerical, integral matrix method[10-12] and there is an existing computer program for the solution called BLIMP.[13]

The boundary-layer equations for an s,y coordinate system of a blunt, axisymmetric body (see Fig. 3) are

Continuity:

$$(1/r_b)\partial(\rho u r_b)/\partial s+\partial(\rho v)/\partial y=0 \tag{27}$$

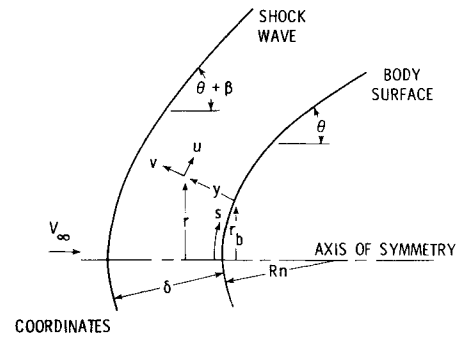

Fig. 3 Flowfield coordinate system for axisymmetric blunt body.

s-momentum:

$$\rho u\frac{\partial u}{\partial s}+\rho v\frac{\partial u}{\partial y}=\frac{\partial}{\partial y}\left[(\mu+\rho\varepsilon_m)\frac{\partial u}{\partial y}\right]-\frac{\partial p}{\partial s} \tag{28}$$

y-momentum:

$$\partial p/\partial y=0 \tag{29}$$

Energy:

$$\rho u\frac{\partial H}{\partial s}+\rho v\frac{\partial H}{\partial y}=-(\partial/\partial y)(q^C+q^R) \tag{30}$$

Species:

$$\rho u\frac{\partial \bar{K}_i}{\partial s}+\rho v\frac{\partial \bar{K}_i}{\partial y}=\frac{\partial}{\partial y}\left(\rho\varepsilon_d\frac{\partial \bar{K}_i}{\partial y}-j_i\right) \tag{31}$$

The complexity of using unequal diffusion coefficients for a multicomponent mixture is reduced by a bifurcation approximation for the binary diffusion coefficients. The bifurcation approximation permits the diffusive flux of element i to be expressed explicitly in terms of properties and gradients of element i and of the system as a whole, but not of other elements. By use of the bifurcation approximation, the diffusional mass flux of element i in the species' conservation equation can be expressed as

$$j_i=-\frac{\rho\bar{D}\mu_2}{\mu_1 M}\left[\frac{\partial \bar{Z}_i}{\partial y}+(\bar{Z}_i-\bar{K}_i)\frac{\partial \ln\mu_2}{\partial y}\right] \tag{32}$$

and the convective heat flux in the energy equation can be expressed by

$$q^C=-\left\{(\rho\varepsilon_m+\mu)\frac{\partial(u^2/2)}{\partial y}+(k+\rho\varepsilon_h c_p)\frac{\partial \bar{T}}{\partial y}+\rho\varepsilon_d\left(\frac{\partial h}{\partial y}-c_p\frac{\partial \bar{T}}{\partial y}\right)+\frac{\rho\bar{D}\mu_2}{\mu_1 M}\left[\frac{\partial \bar{h}}{\partial y}-c_p\frac{\partial \bar{T}}{\partial y}+(\bar{h}-h)\frac{\partial \ln\mu_2}{\partial y}\right]\right\} \tag{33}$$

where

$$\left.\begin{aligned}&\bar{h}=\sum Z_j h_j \quad Z_j=M_j\bar{x}_j/F_j\mu_2 \quad \bar{Z}_i=\sum\alpha_{ij}Z_j\\&\bar{c}_p=\sum Z_j c_{p_j} \quad \mu_1=\Sigma\bar{x}_j F_j \quad \mu_2=\sum M_j\bar{x}_j/F_j\end{aligned}\right\} \tag{34}$$

The subscript j refers to species and the subscript i refers to elements. The quantity α_{ij} is the mass fraction of element i in species j and Z_j is a quantity which for unequal diffusion lies between a mass fraction and a mole fraction for species j.

The turbulent transport terms in the equations are expressed in the Boussinesq form of eddy viscosity, eddy diffusion, and eddy conductivity. If turbulent transport is considered, the turbulent transport properties are included in the boundary-layer equations when a prespecified Reynolds number is exceeded. The Reynolds number is based on edge properties and momentum thickness. A transition region between laminar flow to turbulent flow is not included.

The rate and elemental mass fractions for the mass injection of the ablation products into the boundary layer can be either prespecified or calculated during a solution for steady-state ablation of a heat shield. The equations for the wall boundary conditions in the boundary-layer solution includes the necessary mass and energy balances for steady-state ablation. Thus, the ablation rate of the heat shield can be calculated as part of the solution for steady-state ablation.

Modifications to the BLIMP program were necessary in the present study to clarify the coupling of radiative heating and to make the boundary-layer edge conditions compatible with the inviscid flowfield.

Radiative Transport Solution

The solution of the radiative transport is for a nongray gas with molecular band, continuum, and atomic line transitions. A detailed frequency dependence of the absorption coefficients is used in the integration over the radiation spectrum and the tangent slab approximation is used for integration over physical space. An existing computer program (RAD/EQUIL)[8,9] is used for the calculation of radiative transport.

The absorption coefficients are calculated in the RAD/EQUIL program and the theoretical expressions, approximations, and experimental data of the various transitions for the species are given in detail in Ref. 8. Transitions of the species N, C, H, O, H^-, C^-, N^-, O^-, H_2, C_2, N_2, O_2, NO, CO, CN, and N_2^+ are considered for the radiative transport.

In the computer program, the radiative heating is separated into heating due to continuum transitions and line transitions. The molecular transitions are treated as an "equivalent" continuum process by a bandless model and are included in the continuum contribution to the radiative flux. The line grouping technique is used for the atomic line transitions. In this technique, the line transitions near a specified frequency value are grouped together and the radiative heating is given as that from the line group, however, each line within the group is treated individually.

The RAD/EQUIL computer program is used for the calculation of the radiative transport through the total layer from the coupling of the boundary layer to the inviscid layer. This is step 3 in the calculation procedure. Also, a modified version of the RAD/EQUIL program is used as a subroutine in the computer program for the radiating, inviscid flowfield solution. The modifications affect neither the method nor the accuracy of the calculations for the radiative transport.

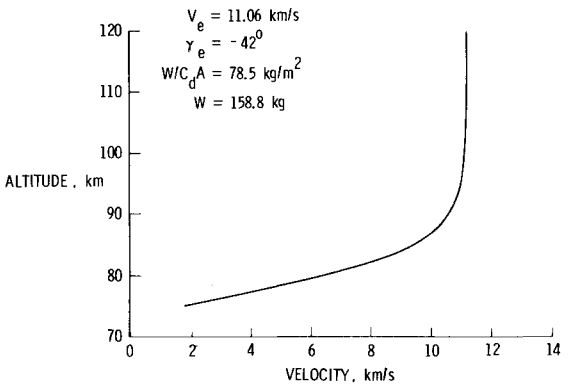

Fig. 4 Trajectory for entry to Venus.

Fully Coupled Solutions for Venusian Entry

The present method was used to obtain solutions at typical conditions for unmanned, scientific probes during Venusian entry. One mission currently under study is a multiprobe entry with one large probe and three small probes which are spherically capped, conical bodies. A description of this type of mission is presented in Refs. 14–17. Results for the large probe are presented in the present paper. (Results for the large probe and a typical small probe are given in Refs. 4 and 18.)

The entry trajectory used in the present analysis for the large probe is presented in Fig. 4. The atmospheric model used for Venus is that presented in Ref. 15 and the gas composition is 97% carbon dioxide and 3% nitrogen by volume. Stagnation-point, radiative heating rates were calculated along the trajectory

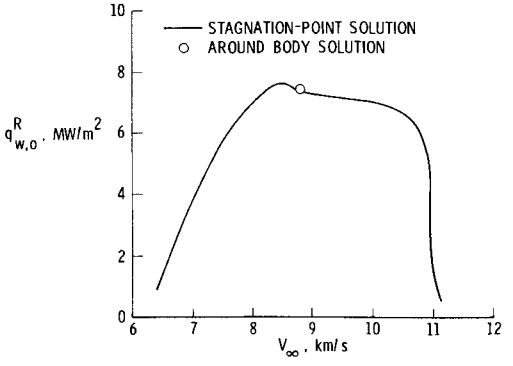

Fig. 5 Stagnation-point, radiative heating rates along entry trajectory.

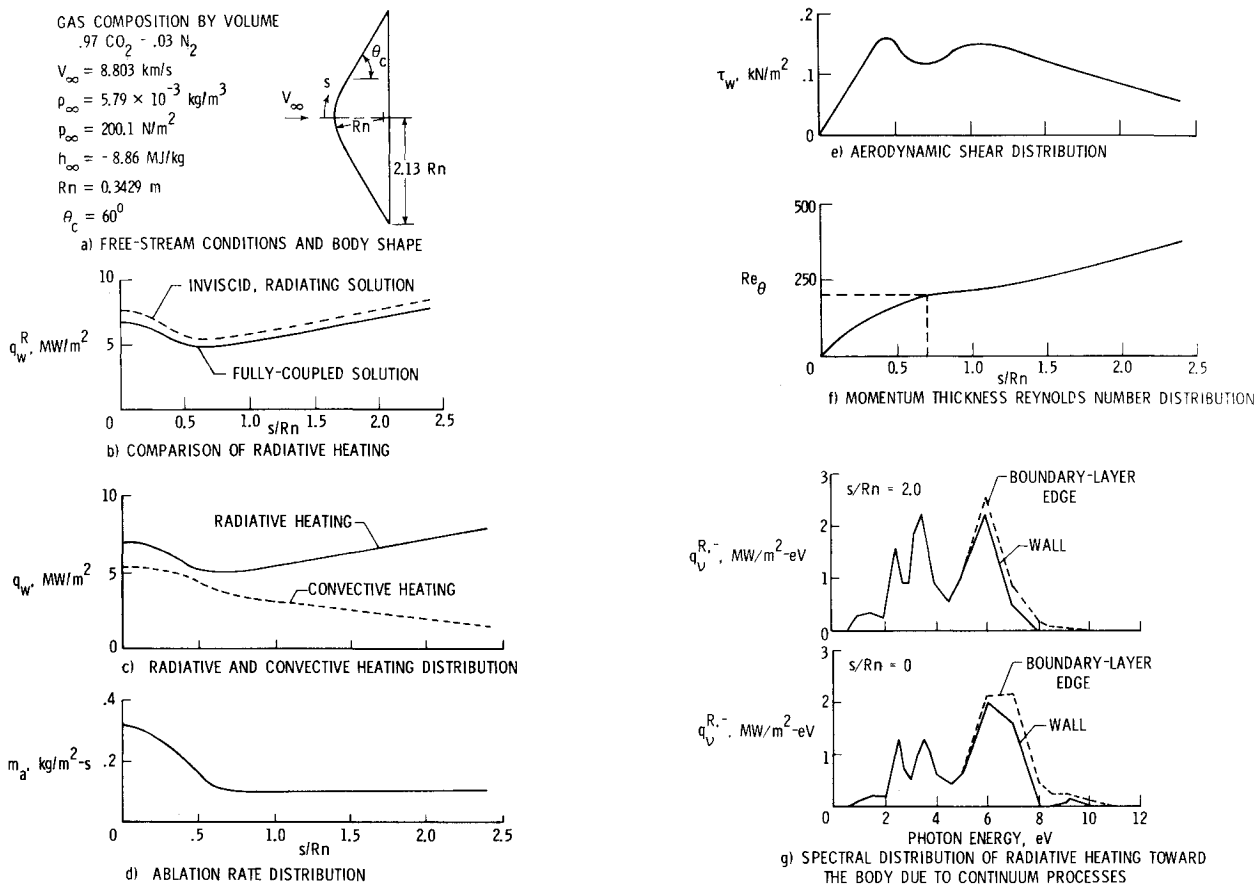

Fig. 6 Fully coupled, radiating flow solution.

to determine the location of peak radiative heating and the results are presented in Fig. 5. A "stagnation-point" version of the developed, radiating inviscid flow program was used for the calculations. The value shown by the symbol in Fig. 5 was chosen as being representative of peak radiative heating and a fully coupled solution with ablation product effects was obtained for the flow around the body at the flight conditions for peak heating. The ablation of the heat shield is represented by steady-state ablation of a carbon-phenolic material with elemental mass fractions of carbon, 0.851; oxygen, 0.110; hydrogen, 0.035; and nitrogen, 0.004. The steady-state ablation rates are obtained as part of the fully coupled solution and are not prespecified.

The results from the fully coupled solution are presented in Fig. 6. The distribution along the body of radiative heating, convective heating, ablation rate, aerodynamic shear, and momentum thickness Reynolds number are presented. The spectral distribution of radiative heat flux due to continuum processes is also presented for two body locations. At this flight condition, the line radiation is small compared to the continuum.

The ablation rate decreases in the nose region and reaches a nearly constant value along the afterbody (Fig. 6d). As shown in Fig. 6c, the convective heating rate decreases along the afterbody but the radiative heating rate increases to values which exceed the stagnation-point value. The radiative heating to the wall is greater than the convective heating along the entire body. The total heating rate, radiative plus convective, along the afterbody is 30% to 40% less than the stagnation-point value. Thus, the decrease in convective heating rate along the afterbody counterbalances the effect of the increase in radiative heating rate. The wall temperature resulting from the steady-state ablation is 3600° K, within 2%, along the entire body and is sufficient for sublimation of the char.

The radiative heating rates from an inviscid, radiating solution are compared with the results for the fully coupled solution with steady-state ablation in Fig. 6b. The radiative heating rates from the fully coupled solution are less than the values from the inviscid, radiating solutions by 9% and this percent reduction is nearly constant along the body. (For a typical small Pioneer Venus probe, the reduction is 17% along the body.[4,18]) The reduction in radiative heating is due to absorption of radiation within the boundary layer.

Spectral distributions of radiative heating toward the body due to continuum processes are presented in Fig. 6g for the stagnation point and an afterbody location. As shown by the results, the absorption of radiation within the boundary layer occurs in the spectral range of 5–10 ev and is due to self-absorption of the fourth positive band system of carbon monoxide, CO(4+). There is a slight increase in radiative heating within the boundary layer at 2.5 ev and this is due to the Swan band system of diatomic carbon, C_2(S); but the effect is too small to be presented in the figures.

Laminar flow in the boundary layer was assumed for this solution. Shown in Fig. 6f is the distribution of momentum thickness Reynolds number around the body. If the critical value for transition to turbulent flow is about 200, then the boundary layer would be turbulent along the afterbody and this could have an appreciable effect on the distribution of convective heating, ablation rate, and aerodynamic shear.

A fully coupled solution with a turbulent boundary layer was obtained and the results are compared with the laminar case in Fig. 7. A critical value of 200 for the momentum thickness Reynolds number was used for transition to turbulent flow. As expected, the convective heating rates, ablation rates, and aerodynamic shears increased with transition to turbulent flow. The distribution of radiative heating along the body was essentially the same for both laminar and turbulent flow; thus, the turbulent boundary layer did not appear to further attenuate the radiative heating even though the boundary-layer thickness was 80% greater than for laminar flow. This phenomenon can be explained with the spectral distributions of radiative flux at the wall

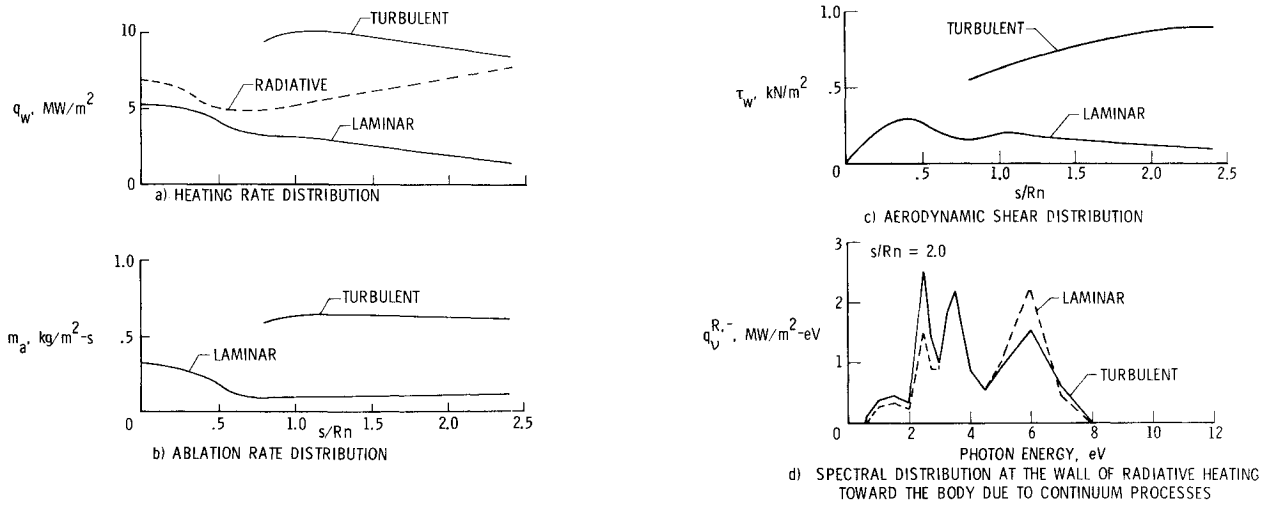

Fig. 7 Comparison between a turbulent and laminar boundary layer for fully coupled solution.

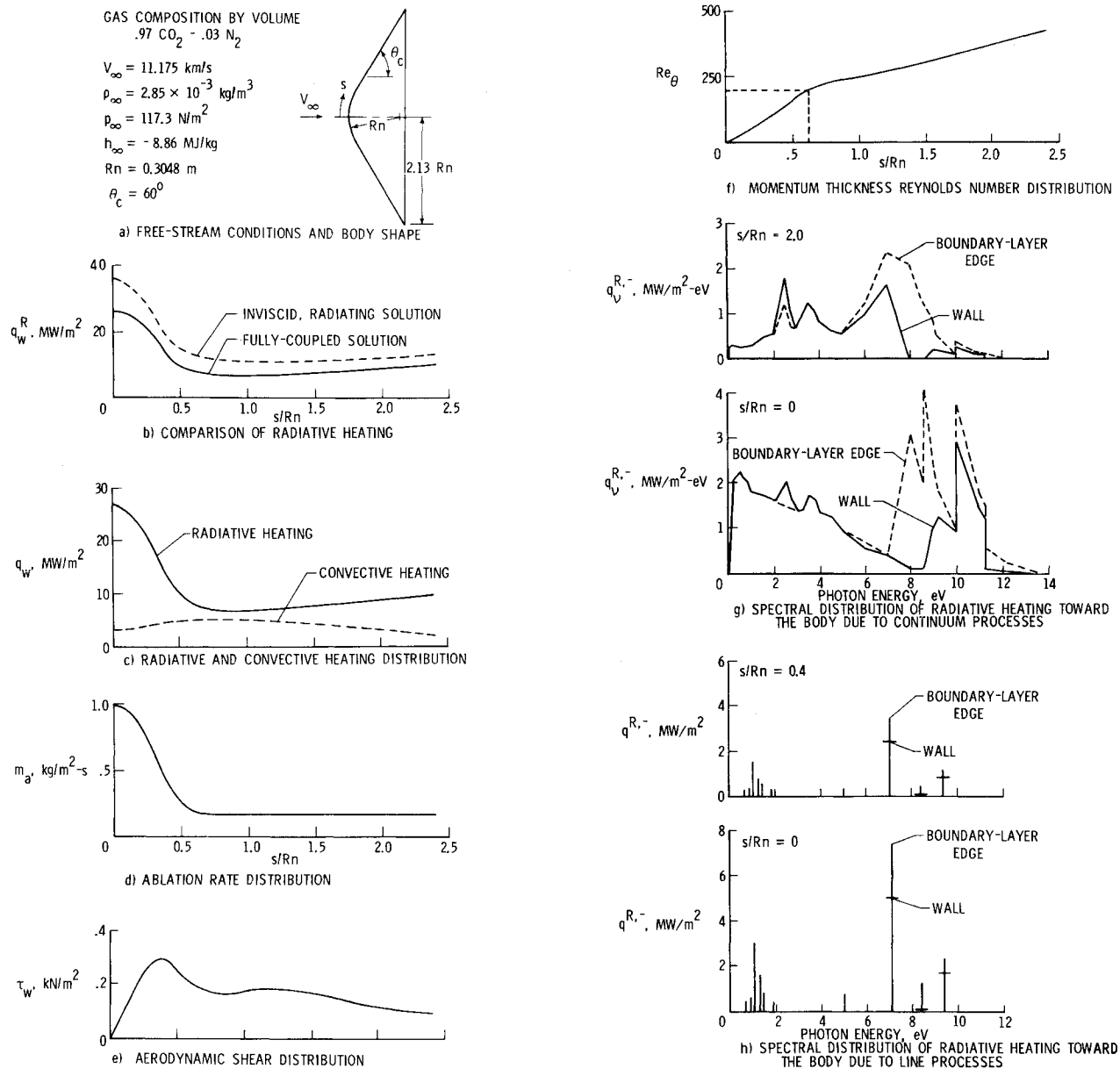

Fig. 8 Fully coupled, radiating flow solution for high velocity entry.

presented in Fig. 7d for the turbulent and laminar solutions. For the turbulent boundary layer, there is an increase in the self-absorption of the CO(4+) band system in the spectral range of 5–8 ev but this effect is offset by an increased emission of the $C_2(S)$ band system at 2.5 ev and the red band system of cyanogen, CN(R), at 0.6 to 2 ev. The spectral distribution at the boundary-layer edge is essentially the same for both the turbulent and laminar boundary layers and was presented in Fig. 6g. While the radiative heating rates along the afterbody are the same for a turbulent or a laminar boundary layer, the wall spectral distribution of the radiation is different for the two cases. It should not be inferred that the radiative heating to the body will be the same for a laminar or turbulent boundary layer for other entry conditions or other body shapes.

A fully coupled solution was obtained for freestream conditions representative of a higher entry velocity than that of the nominal trajectory and the results are presented in Fig. 8. The freestream conditions and body shape are given in Fig. 8a. Hereafter, this case is referred to as the high velocity entry.

As shown in Fig. 8c, the radiative heating rate is greater than the convective heating rate along the entire body. Unlike the results previously presented, there is only a slight increase in the radiative heating along the afterbody. The convective heating rate at the stagnation point is slightly less than the value just downstream of the stagnation point. This is due to an increased effect of blockage of convective heating by the mass injection of the ablation products. As shown in Fig. 8d, the ablation rate decreases along the body in the nose region. The ablation rate and total heating rate are nearly constant along the afterbody. The wall temperature resulting from the steady-state ablation is 3750° K, within 1%, along the body and is sufficient for sublimation of the char.

There is significant absorption of radiation within the boundary layer for the high velocity entry as shown by a comparison of results between the fully coupled solution and an inviscid, radiating solution in Fig. 8b. The reduction in radiative heating rate is 25% at the stagnation point and 25% to 30% along the afterbody. Spectral distributions of radiative heating toward the body due to continuum processes are presented in Fig. 8g for the stagnation point and an afterbody location. For the continuum processes, most of the absorption within the boundary layer occurs in the spectral region of 5–10 ev and is due mainly to self-absorption of the CO(4+) band. There is an increase in radiative flux at 2.5 ev and this is due to the $C_2(S)$ band. At the stagnation point there is absorption at photon energies greater than 10 ev and this absorption is attributed to atomic species within the cooler regions of the boundary layer. There is also absorption at the photoionization edge of carbon at 8.5 ev.

The radiative flux due to line processes is 50% of the total radiative flux at the nose region of the body and decreases to only 20% along the afterbody. Spectral distributions of the radiative heating due to line processes for two locations at the nose region are presented in Fig. 8h. Absorption of line radiation within the boundary layer occurs only for the line groups in the ultraviolet at 7.1, 8.4, and 9.4 ev. The line radiation in the visible and infrared regions of the spectrum, less than 2 ev, is not attenuated within the boundary layer.

Conclusions

A method of solution for the fully coupled radiating gas flow about an ablating planetary entry body is developed and applied to Venusian entries. The method couples an inviscid flow solution and a boundary-layer solution (laminar or turbulent) in which the divergence of the radiative flux is included in the energy equation for the solution of each gas layer. The treatment of radiation includes molecular band, continuum, and line transitions with a detailed frequency dependence of the absorption coefficient. Results are presented at typical conditions for unmanned, scientific probes during Venusian entries. These results show that the radiative flux toward the body is attenuated in the boundary layer at downstream regions of the body as well as at the stagnation point, and that, even when radiation absorption by ablation products is accounted for, the radiative heating rates along the downstream regions of the body can, under certain conditions, exceed the stagnation-point values. It is also shown that, for Venusian entry, the spectral distribution of radiative flux and the magnitude of radiation absorption by ablation products depend strongly on entry velocity, and that the state of the boundary layer (i.e., laminar or turbulent) can significantly influence the amount of ablation product absorption or emission that occurs in various spectral regions.

The attenuation of radiation by the boundary layer will reduce the radiative heating to the body by 10%–20% at entry conditions and body shapes which are presently considered as nominal for unmanned, Venusian entries. The reduction can be as large as 30% at higher velocity entries.

References

[1] Garrett, L. B., Smith, G. L., and Perkins, J. N., "An Implicit Finite-Difference Solution to the Viscous Shock Layer, Including the Effects of Radiation and Strong Blowing," TR R-388, 1972, NASA.

[2] Page, W. A., "Aerodynamic Heating for Probe Vehicles Entering the Outer Planets," AAS Paper AAS-71-144, 1971, American Astronautical Society, Seattle, Wash.

[3] Callis, L. B., "Coupled Nongray Radiating Flows about Long Blunt Bodies," *AIAA Journal*, Vol. 9, No. 4, April 1971, pp. 553–559.

[4] Sutton, K., "Characteristics of Coupled Nongray Radiating Gas Flows with Ablation Product Effects about Blunt Bodies During Planetary Entries," Ph.D. thesis, 1973, Dept. of Mechanical and Aerospace Engineering, North Carolina State University at Rayleigh, Rayleigh, N.C.

[5] MacCormack, R. W., "The Effect of Viscosity in Hypervelocity Impact Cratering," AIAA Paper 69-354, Cincinnati, Ohio, 1969.

[6] MacCormack, R. W., "Numerical Solution of the Interaction of a Shock Wave With a Laminar Boundary Layer," *Proceedings of the Second International Conference on Numerical Methods in Fluid Dynamics*, edited by M. Holt, Springer-Verlag, New York, 1970, pp. 151–163 (see Vol. 8 in *Lecture Notes in Physics*).

[7] Callis, L. B., "Solutions of Blunt-Body Stagnation Region Flows with Nongray Emission and Absorption of Radiation by a Time-Asymptotic Technique," TR R-399, 1969, NASA.

[8] Nicolet, W. E., "Advanced Methods for Calculating Radiation Transport in Ablation-Product Contaminated Boundary Layers," CR-1656, 1970, NASA.

[9] Nicolet, W. E., "User's Manual for the Generalized Radiation Transfer Code (RAD/EQUIL)," Aerotherm Rept. UM-69-9, 1969, Aerotherm Corp., Mountain View, Calif., available as CR-116353, NASA.

[10] Bartlett, E. P. and Kendall, R. M., "An Analysis of the Coupled Chemically Reacting Boundary Layer and Charring Ablator. Pt. III—Nonsimilar Solution of the Multicomponent Laminar Boundary Layer by an Integral Matrix Method," CR-1062, 1968, NASA.

[11] Kendall, R. M. and Bartlett, E. P., "Nonsimilar Solution of the Multicomponent Laminar Boundary Layer by an Integral-Matrix Method," *AIAA Journal*, Vol. 6, No. 6, June 1968, pp. 1089–1097.

[12] Kendall, R. M., Anderson, L. W., and Aungier, R. H., "Nonsimilar Solution for Laminar and Turbulent Boundary-Layer Flows over Ablating Surfaces," *AIAA Journal*, Vol. 10, No. 9, Sept. 1972, pp. 1230–1236.

[13] Anderson, L. W. and Morse, H. L., "User's Manual—Vol. I—Boundary Layer Integral Matrix Procedure (BLIMP)," TR AFWL-TR-69-114, Vol. I (Suppl.), 1971, Air Force Weapons Laboratory, Kirtland Air Force Base, N. Mex.

[14] "Venus, Strategy for Exploration," Report of a Study by the Space Science Board, 1970, National Academy of Sciences, Washington, D.C.

[15] "Pioneer Venus," Report of a Study by the Science Steering Group, 1972, NASA.

[16] Ainsworth, J. E., "Comprehensive Study of Venus by Means of a Low-Cost Entry-Probe and Orbiter Mission-Series," Rept. X-625-70-203, 1970, Goddard Space Flight Center, Greenbelt, Md.

[17] Marcotte, P. G., "Planetary Explorer, Phase A Report and Universal Bus Description," TM X-65423, 1971, NASA.

[18] Sutton, K., "Fully Coupled Nongray Radiating Gas Flows With Ablation Product Effects About Planetary Entry Bodies," AIAA Paper 73-672, Palm Springs, Calif., 1973.